

Alginate Supramolecular Hydrogels Based on Viologen and Cucurbit[8]uril: Host-Induced Caveolae-Mediated Endocytosis to White Blood Cancer Cells

Falguni Chandra¹, Marya Bykova², Vijo Polous¹, Paltan Laha¹, Alina Aktanova², Olga Boeva², Margarita Barkovskaya², Ekaterina Pashkina², and Na'il Saleh³

¹United Arab Emirates University

²Novosibirskij gosudarstvennyj medicinskij universitet Ministerstva zdravoohranenia Rossijskoj Federacii

³UAE University

July 17, 2023

Abstract

The cellular uptake of drug carriers to the cytosol of a specific cell remains challenging, and a non-classical supramolecular strategy is motivated. Here, we select a model host-guest complex in which a diamino-viologen (VG) fluorescent tag was engulfed by cucurbit[8]uril (CB8) and covalently linked to alginate polysaccharides (ALG) as the modified drug vehicle. When adsorbed on the ALG surface, the encapsulation of VG was first confirmed utilizing FTIR and NMR spectroscopic methods. Solid optical measurements (DRS, PL, and TRPL) revealed emissive materials at around 650 nm and that CB8 enhanced the rigidity of the modified hydrogel. The molar composition of 2 to 1 for the complexation of VG to CB8 on the alginate surface and the thermal stabilities were also confirmed using TGA and DSC techniques. CB8 induced a dramatic decrease in the average size of the VGALG polysaccharides from 485 to 165 nm and a turnover in their charge from -19.8 to +14.4 mV. Flow cytometry with inhibitors of various endocytosis pathways was employed to track the cellular uptake across different blood cell types: human T-cell leukemia 1301 and peripheral blood mononuclear cells. Noticeably, complexation of VG to CB8 host on top of the sugar platform dramatically enhanced the internalization to 1301 cells (viz. from 1 to 99%) at a concentration of 1.8 mg/mL via caveolae-mediated endocytosis (CvME) because of the size reduction, turnover in the charge from negative to positive, and rigidity induction. These observations reveal a more profound understanding of the macrocyclic effects on drug delivery

Alginate Supramolecular Hydrogels Based on Viologen and Cucurbit[8]uril: Host-Induced Caveolae-Mediated Endocytosis to White Blood Cancer Cells

Falguni Chandra,^{+§} Maria Bykova,⁺⁺ Vijo Polous,⁺ Paltan Laha, ^{+SS} Alina Aktanova,^{++[?]} Olga Boeva,⁺⁺ Margarita Barkovskaya, ⁺⁺ Ekaterina Pashkina,^{*,++[?]} and Na'il Saleh^{*+SS}

⁺Department of Chemistry, College of Science, United Arab Emirates University, P.O. Box 15551, Al Ain, United Arab Emirates

^{SS}Zayed Bin Sultan Center for Health Sciences, United Arab Emirates University, PO. Box 15551 Al Ain, United Arab Emirates

⁺⁺Laboratory of Clinical Immunopathology, Research Institute of Fundamental and Clinical Immunology, 14 Yadrintsevskaya, 6300099 Novosibirsk, Russia

^[?]Novosibirsk State Medical University, 52, Krasny Prospect, 630091 Novosibirsk, Russia

*Corresponding and submitting author: n.saleh@uaeu.ac.ae (N.S.). Tel.: +971-(0)3-713-6138, eapashkina@niikim.ru (E.P.) Tel.: +7923-190-4706

ABSTRACT. The cellular uptake of drug carriers to the cytosol of a specific cell remains challenging, and a non-classical supramolecular strategy is motivated. Here, we select a model host-guest complex in which a diamino-viologen (VG) fluorescent tag was engulfed by cucurbit[8]uril (CB8) and covalently linked to alginate polysaccharides (ALG) as the modified drug vehicle. When adsorbed on the ALG surface, the encapsulation of VG was first confirmed utilizing FTIR and NMR spectroscopic methods. Solid optical measurements (DRS, PL, and TRPL) revealed emissive materials at around 650 nm and that CB8 enhanced the rigidity of the modified hydrogel. The molar composition of 2 to 1 for the complexation of VG to CB8 on the alginate surface and the thermal stabilities were also confirmed using TGA and DSC techniques. CB8 induced a dramatic decrease in the average size of the VGALG polysaccharides from 485 to 165 nm and a turnover in their charge from -19.8 to +14.4 mV. Flow cytometry with inhibitors of various endocytosis pathways was employed to track the cellular uptake across different blood cell types: human T-cell leukemia 1301 and peripheral blood mononuclear cells. Noticeably, complexation of VG to CB8 host on top of the sugar platform dramatically enhanced the internalization to 1301 cells (viz. from 1 to 99%) at a concentration of 1.8 mg/mL via caveolae-mediated endocytosis (CvME) because of the size reduction, turnover in the charge from negative to positive, and rigidity induction. These observations reveal a more profound understanding of the macrocyclic effects on drug delivery.

KEYWORDS: Cucurbiturils, alginates, viologen, time-resolved photoluminescence, cellular uptake, blood cancer cells.

INTRODUCTION

Optimizing drug-delivery methods to improve immunotherapeutic efficiency is often aided by different strategies that modulate cell or tissue targeting, controlled release, and the response of the drug to suitable triggers.^[1]

Using a dynamic host-guest system, the supramolecular scientists set their goals by providing specific, tunable, and thermodynamically reversible bonds. This concept also led them to develop water-soluble nanocontainer-based drug delivery systems such as cucurbituril (CB)-based drug-delivery systems.^[2] Nature is the primary inspiration for studying supramolecular chemistry in biorecognition, which includes multi-molecular host-guest complexes formed by noncovalent interaction between suitable complementary guest molecules and nanocavity-based macrocyclic molecules known as molecular recognition.^[3]

The reversible associations are highly selective and have been employed over several decades in generating supramolecular hydrogels such as polysaccharides-based hydrogels.^[4,5] Generally, supramolecular hydrogels' excellent elastic and mobility nature^[6] offers superior performance in biomedical applications over chemically crosslinked. UV light-induced crosslinking or in situ crosslinking can irreversibly generate the latter. Yet, the resulting covalently crosslinked hydrogels are rigid and brittle and cannot be tuned. Due to several dynamic physical bonding and a shorter time for gelation formation, the supramolecular hydrogels gained unique properties such as excellent shear-thinning^[7] elasticity,^[8] mouldability, sol-gel switching,^[9] capability for self-healing,^[10] and control release of growth factors. The supramolecular hydrogels are known to have a well-defined stoichiometry, contiguous network, and high biocompatibility due to their high selectivity and supercilious binding strength.^[11] The external environmental biochemical and physical variation can regulate the reversible association and dissociation of the host-guest supramolecular system.^[12] Also, supramolecular hydrogels can be tailored for application *in vivo* due to their significant water content and biocompatibility.^[13] Specifically, employing supramolecular hydrogels based on polysaccharides for biomedical applications utilizing CB macromolecules is not original.^[5] It has also been described for various biological and clinical applications. For instance, biomedical researchers reported different designs using CB for crosslinking the supramolecular hydrogel based on various functional tags. Yet, the exact mechanism of cellular uptake by macrocycle-based hydrogels is to be explored.

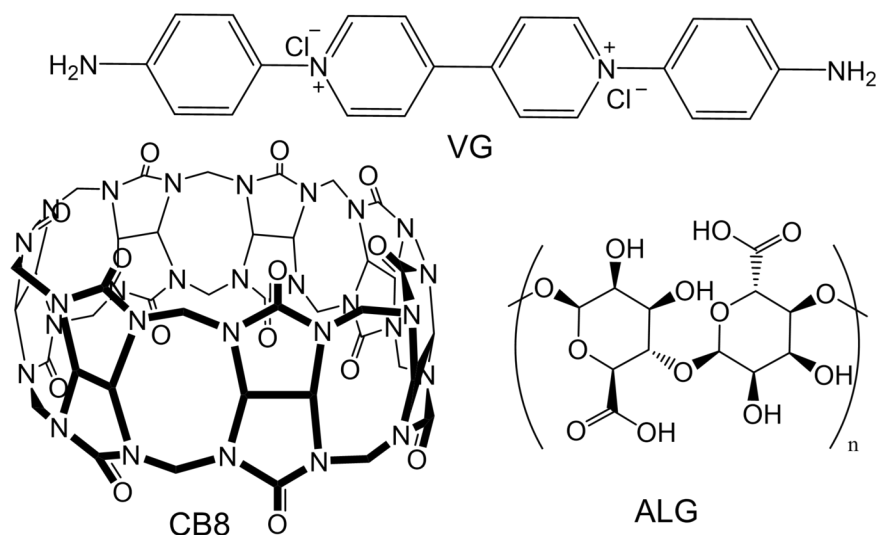
Nowadays, treating and curing cancer is the world's most pressing health-challenging task for clinical research.

According to the WHO estimation, cancer death will increase globally by 80% by 2030.^[14] On a global level, seven out of ten cancer deaths happened in Asia, Africa, Central and South America.^[15] Leukemia is the most challenging treatment among all types of cancer. Clinical scientists are continuously working hard to prevent this grim projection. With care that aims to balance the effectiveness of treatment and the importance of quality of life, more patients than ever are living longer.

The nanocavity cucurbit[*n*]urils (CB_{*n*}) are more biocompatible than other water-soluble macrocyclic hosts because CB_{*n*} is dexterity to functionalization.^[16] The water-soluble macrocyclic molecules offer their hydrophobic cavity for encapsulating polar and non-polar guest molecules with a reasonable binding constant.^[17] CB_{*n*} is made from acid-catalyzed polymerization of glycoluril and formaldehyde to form macrocycles with different numbers of monomers unit.

The eight-monomer unit containing cucurbit[8]uril (CB8) forms a complex with viologen guests non-covalently.^[18] The viologens are functional organic materials first discovered by Michaelis in 1932.^[19] The viologens are the classic example of redox and electron-deficient compounds. Several viologen-based crystalline and amorphous photochromic materials have been synthesized for the last ten years, enabling photochemists to develop substantial multifunctional viologen-based photochromic materials.^[20] To be effective, precise structural control of such materials is required. This, of course, puts a premium on the ability to control structural parameters during their tedious synthesis. However, the precise structural control of hydrogels is not easy. It requires the simultaneous adjustment of several parameters and/or possibly different processing techniques to achieve any size, charge, or rigidity.

Here, a supramolecular hydrogel as a drug delivery system is designed in which CB8-encapsulated viologen diamines salts (VG)^[21] are covalently linked to the surface of alginate polysaccharides (ALG)^[22] (Figure 1).



All starting reagents cucurbit[8]uril (CB8), 1,1'-bis(4-aminophenyl)-[4,4'-bipyridine]-1,1'-dium dichloride (VG), alginic acid (ALG), 4-dimethylamino pyridine (DMAP), and N,N'-dicyclohexylcarbodiimide (DCC), as well as methanol and DMSO solvents, including the deuterated ones, were obtained from Sigma-Aldrich (St. Louis, MO) and used as received. All chemicals had purities exceeding 95%, except for CB8, which was assumed to contain 20% (w/w) water in the supplied bottles.

Preparation of VGALG and VGCB8ALG Conjugate .

ALG (0.41 g), DCC (0.08 g, 0.38 mmol), and DMAP (0.051 g, 0.42 mmol) were dissolved in dimethyl sulfoxide (DMSO), purged under nitrogen for one hour at 295 K (50 mL), and the solution was stirred for sixteen hours. A 1:1 mixture (0.032 mmol) of VG and CB8 was dissolved in DMSO/ water (20 mL, 1:1 v/v) in a separate flask with six hours of stirring under nitrogen at 298 K. The two solutions were mixed and stirred for two hours under nitrogen at 328 K and then purified by dialysis against water (pH 7) for several days to separate the solid conjugates from unreacted starting materials. The final suspension was centrifuged for eight hours, and the solid product was washed with water and freeze-dried for ten hours.

Fourier Transform Infrared (FTIR) Spectroscopy.

The FTIR spectra were recorded on a Perkin Elmer spectrometer, and the data were processed with Spectrum IR software. The solid samples were mixed with dry KBr (FT-IR grade Sigma-Aldrich, St.Louis, MO) in a ratio of 1:100 and compressed into pellets using a hydraulic press. The resulting pellet's transmittance was recorded within a range of 4000–450 cm^{-1} with thirty-two scans.

Proton Nuclear Magnetic Resonance (NMR) Spectroscopy.

Proton NMR spectra were recorded on a 400 MHz Varian spectrometer (Varian, Inc., Palo Alto, CA), all the measurements were done in DMSO- d_6 solvent, and all the peaks were referenced to residual protonated solvent with chemical shift (δ) =2.49 ppm.

Thermogravimetric Analysis (TGA).

Thermogravimetric analysis was conducted on a Mettler Toledo thermal analyzer (TGA 2, Switzerland). All solid samples were measured in the 25–600 °C temperature range at a heating rate of 10 °C/min under the gaseous nitrogen flux, and the data was processed with STAR software.

Differential Scanning Calorimetry (DSC).

The differential scanning calorimetric measurements were recorded on a Shimadzu DSc-60 Plus (DSC instrument, Japan). The software workstation LabSolutions TA controlled thermal analysis. The sample was precisely weighed on a microbalance taken on an aluminum crimp pan with a top lid. All samples were measured in the 25–400 °C temperature range at a heating rate of 10 °C/min under a constant nitrogen flow of 100 mL/min.

Size Distribution and Zeta Potential Analysis.

The particle size (z-average d.nm) and ζ potential (mV) were recorded on a Malvern zetasizer Nano ZS instrument (Malvern Instruments UK). All solid samples dispersed in methanol (Honeywell HPLC grade) [?] 0.1 mg/mL concentration, vortexed and analyzed by using a disposable sizing cuvette for DLS measurement and electrophoretic measurement were performed on a zetasizer cell at 25 °C after 120 seconds temperature equilibration at a backscattering angle of 173°.

Diffuse Reflectance Spectroscopy (DRS).

The absorption spectra of the solid samples were obtained by using the Kubelka–Munk conversion ($K-M = (1 - R)^2/2R$) of the recorded diffusive-reflectance spectra at room temperature for the solid samples on an FS5 spectrometer (Edinburgh, UK) equipped with an SC-30 (integrating sphere) as the sample holder. The specular reflection of the sample surface light was removed from the signal by directing the incident light at the sample at an angle of 0°; only the diffusive reflected light was measured. Polytetrafluoroethylene

(PTFE) polymer was used as the reference. The bandgap energy (E_g) values of the solid samples from the DRS spectra were calculated using $E_g = 1240 \text{ eV nm l}^{-1}$, where l is the absorption edge (in nm).

Photoluminescence (PL) and Photoluminescence-Excitation (PLE) Measurements .

Fluorescence spectra were recorded on a spectrofluorometer FS5 instrument (Edinburg, United Kingdom) using slit widths of 2.0 nm for both the excitation and the emission monochromators in all experiments. The estimated experimental error was 2% for a lifetime value of less than one ns and 20% for a lifetime of around five ns.

Excited-State PL Lifetime Measurements and Time-Resolved Photoluminescence (TRPL) Measurements.

The time-resolved photoluminescence measurements were performed on a LifeSpec-II spectrometer (Edinburgh Inc., Edinburgh, United Kingdom) based on the Time-Correlated Single Photon Counting (TCSPC) method. The excitation diode laser source was set at 475 nm and used on an Edinburgh instrument (Edinburgh Inc., Edinburgh, United Kingdom) with a repetition rate of 20 MHz, a time resolution of 30 ps, and a red-sensitive high-speed photomultiplier tube detector (Hamamatsu, H5773-04). The data were analyzed by the iterative reconvolution method using the instrument's software that utilizes the Levenberg–Marquardt algorithm to minimize χ^2 . The fluorescence decay was analyzed in terms of the multi-exponential model to calculate the average lifetime value, given by:

$$\tau = \sum_i f_i \tau_i \quad (1)$$

And the contribution of each component to the steady-state intensity is given by:

$$f_i = \frac{\alpha_i \tau_i}{\sum_j \alpha_j \tau_j} \quad (2)$$

Where τ_i are the lifetimes with amplitudes α_i and $\sum_i \alpha_i \tau_i = 1.0$. And the sum in the denominator is for all the decay times and amplitudes.

Medicinal Research Materials.

Human T-cell leukemia cell line 1301 (European collection of authenticated cell cultures, Sigma Aldrich, Merck KGaA, Germany) and Peripheral blood mononuclear cells (PBMCs) from healthy donors ($n = 7$) were used as the material for the study. The ethics committee of RIFCI, Russia, approved the design of the study and recruitment of donors. Donors gave written informed consent.

PBMCs Isolation.

PBMCs were isolated from the heparinized venous blood of healthy donors using the ficoll-urografin (1.077 g/mL) density gradient centrifugation method. The fresh heparinized venous blood (5 ml) was layered into a test tube for 3 mL ficoll-urografin (1.077 g/mL). The tubes were centrifuged for 20 minutes at 2700 rpm. After centrifugation, mononuclear rings were collected into separate tubes, followed by double washing in 10 mL of phosphate-buffered saline (PBS) end ethylenedinitriлотetraacetic acid disodium salt dihydrate Na_2EDTA 1%. The washed cells were placed in 1 mL of RPMI-1640 (Gibco, Invitrogen, Carlsbad, CA, USA). Then they were counted using the Goryaev camera.

Cultivation.

Cells at a concentration of 1 million/mL (PBMCs) or 150,000 cells/ml (1301 cell line) were cultured for 1, 24, or 72 hours in 96-well plates (in a volume of 100 μL) in RPMI-1640 medium (Gibco, Cat. No. 27016021) containing 0.3% L-glutamine, 50 $\mu\text{g/mL}$ gentamicin, 25 $\mu\text{g/mL}$ of thienam and 10% inactivated fetal calf serum (FCS) (Hyclone, Chicago, IL, USA) in the presence of various concentrations of VGALG and VGCB8ALG (1.8 mg /mL; 0.18 mg/mL; 0.018 mg/ mL; 0.0018 mg/mL; 0 mg/mL).

Cytotoxicity of Hydrogels.

The cytotoxicity of hydrogels was evaluated using WST-1 assay kit (Takara Bio, Kusatsu, Japan) and LDH-Cytox Assay Kit (BioLegend, San Diego, CA, USA). Ten μL WST-1 was added to the cell culture

media and incubated for four hours at 37°C in the incubator. As a positive control, 10% DMSO was used. The cytotoxicity of VGALG and VGCB8ALG was analyzed by the amount of formazan dye produced by measuring the absorbance at 450 nm. To perform the lactate dehydrogenase (LDH) assay for the cellular cytotoxicity of the compounds, the reaction mixture was added to the wells of the cell culture medium. After 30 min of incubation with lysis buffer and 30 min of incubation with assay buffer with protection from light, the reaction was stopped by adding a stop solution, and the absorbance was measured using a microplate reader Infinite F50 (Tecan, Grödig, Austria) at 490 nm. The average absorbance of each triplicate set of wells was calculated, and the background control value was subtracted. The percent cytotoxicity was calculated with the following equation:

$$\text{Cytotoxicity}(\%) = \frac{A-C}{B-C} \times 100 \quad (3)$$

where A: Test Substance, B: High Control, C: Low Control.

Internalization.

After cultivation, the cells were collected, and PBMCs were labeled with surface markers using anti-CD3-FITC and anti-CD14-APC antibodies (all Biolegend, San Diego, CA, USA). Internalization was determined by the modified viologen in the composition of hydrogels, whose fluorescence spectrum was shifted to longer wavelengths and was detected by flow cytometry (Ex 488 nm, Em 695 nm). Internalization evaluation was performed cytometrically using flow cytometry (BD FACSCanto II cytometer) and FACSDiva software (Becton Dickinson, Franklin Lakes, NJ, USA). Further, to establish the uptake route of hydrogels, 1301 cells were exposed to various pharmacological inhibitors, including methyl-beta-cyclodextrin (M β CD), chlorpromazine, nystatin, N-ethylisopropylamiloride (EIPA), dynasore, cytochalasin or wortmannin, in the 12-well plates at the concentration of 150,000 cells/mL for one hour. Later, the hydrogels (0.18 mg/mL) were added and co-incubated for an additional hour. Here was another group with a low temperature. 1301 cells were precooled at 4 for 30 minutes, and then, the treatment was the same as the previous four inhibitor groups but at 4 all the time. As for the flow cytometry analysis, the cells were harvested using centrifugation, then washed twice and made into a single-cell suspension for flow cytometry analysis. 10000 events were collected for each sample.

Fluorescence Microscopy.

The cellular uptake of hydrogels was investigated by fluorescence microscopy. Cells were incubated with VGCB8ALG or VGALG (0.18 mg/mL) for 24 hours. Then, cells were washed twice with 2 mM EDTA solution in PBS and fixed with a mixture of ethanol: glacial acetic acid (3:1, v/v). Cells were resuspended thoroughly to avoid clumps after the fixation step and placed on slides. Then, the slides were analyzed using phase-contrast microscopy for cell cytoplasm and nuclei visualization in transmitted light. After that, slides were mounted with a Pro Long Gold antifade containing 6-diamidino-2-phenylindole (DAPI) (Invitrogen MP, Waltham, MA, USA) to prevent dye photo-bleaching and identify cell nuclei further. Phase-contrast and fluorescent microscopy was performed with the Axioscope 40 fluorescence microscope (Zeiss, Germany). DAPI-stained nuclei images and hydrogel signals were captured separately with the software package ZEN-2012 (Zeiss, Germany) on the magnitude X1000. Exposure time was adjusted automatically.

Statistical data.

Analysis was performed using GraphPad Prism 9.3.1 using Friedman's test using Dunn's test for multiple comparisons. A p value <0.05 was considered the minimum criterion for statistical significance.

RESULTS AND DISCUSSION

Material Characterizations of Hydrogels (Functionalization, Encapsulation, Stoichiometry, Composition, Thermal Stability, Size Distribution, and Charges)

The FTIR spectra of the modified hydrogels in Figure 2 show distinct, entirely different stretching and bending bands compared to those peaks of ALG and VG starting materials (Table S1 in the Supporting

Information) or to the previously reported FTIR spectrum of CB8^[24] confirming the formation of VGALG and VGCB8ALG.

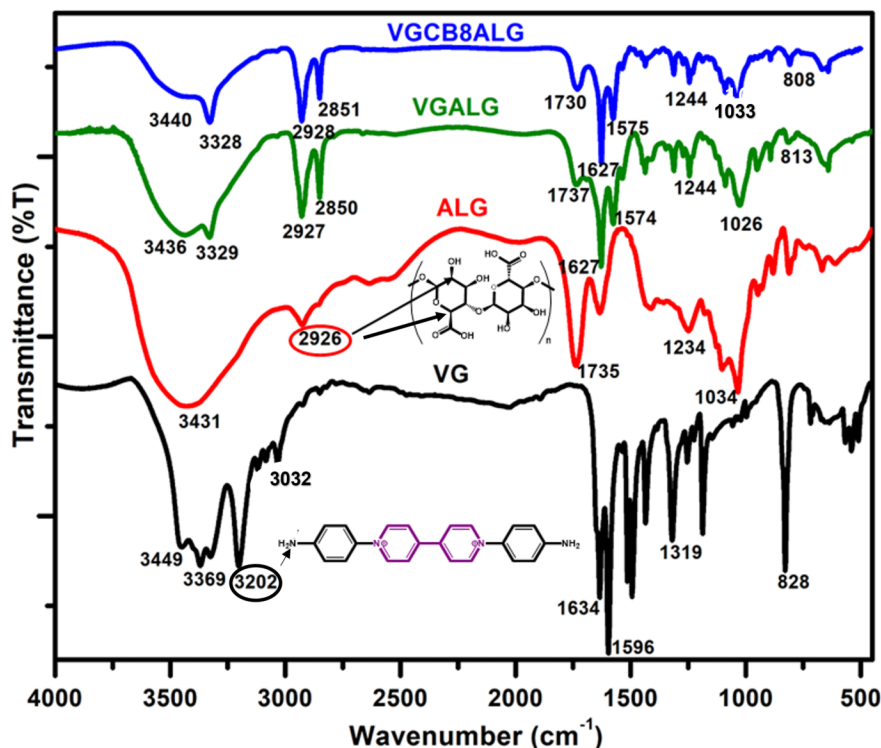


Figure 2. FTIR spectra of VG, ALG, VGALG, and VGCB8ALG hydrogels in KBr solids.

Notably, the peak for (NH₂) primary amine stretching^[21] at 3202 cm⁻¹ and bending at 1634 and 1596 cm⁻¹ (in VG) has evolved into the amide (CONH) peak at 3329 cm⁻¹ and 1627 and 1574 cm⁻¹, respectively (in the modified ALG). Moreover, a significant enhancement in the intensity of the CH stretching (in ALG)^[22] at 2927 and 2850 cm⁻¹ was observed upon its covalent modification by VG or VGCB8. The two FTIR spectra measured for VGALG and VGCB8ALG hydrogels were similar because encapsulation by CB8 does not usually affect the vibration of the guest molecule's bonds.^[24] Only peaks in the range from 1500 to 1400 cm⁻¹ due to the stretching vibration of the benzene rings of VG were slightly weakened.^[24]

In the proton NMR spectra (aromatic region), ALG shows a single broad resonance peak at $\delta = 12.30$ ppm associated with the -OH group in ALG (Figure S1 in the Supporting Information). The NMR spectrum for VG shows five peaks, including one singlet $\delta = 5.30$ ppm (for -NH₂) and four doublets with resonances at $\delta = 6.0, 6.75, 8.2,$ and 8.75 ppm.^[25-27] A new peak at $\delta = 12.25$ ppm appears when VG is linked to ALG due to forming an amide linkage in the VGALG complex with a concomitant shift to lower ppm and broadening of peaks b-e. As expected in similar reports, the peaks b-e of the new hydrogels were further broadened (almost disappeared) upon engulfing VG in CB8.^[26] As additional evidence for the non-covalent entrapment of VG by CB8 in DMSO solution, we measured the UV-Visible absorption spectra of all alginate samples. We noticed several isosbestic points at 250, 300, and 550 nm (Figure S2 in the Supporting Information) in the spectra of the VG-modified ALG in the absence and presence of CB8. The addition of CB8 also shifts the absorption peaks from 245 and 475 nm to 250 and 490 nm, respectively. Additionally, the data served us to confirm the covalent conjugation of VG to ALG by the emergence of new peaks at 245 (250 with CB8), 275, and 475 nm (490 with CB8).

Figure 3 shows the TGA of VG, CB8, ALG, VGALG, and VGCB8ALG in the temperature range from

35°C to 600°C at a heating rate of 10°C. The traces provide information about the composition and thermal decomposition of the new hydrogels VGALG and VGCB8ALG compared to individual viologen and unmodified alginate samples.^[28] More importantly, the results confirm the host-guest interaction between VG and CB8 on the ALG platform.

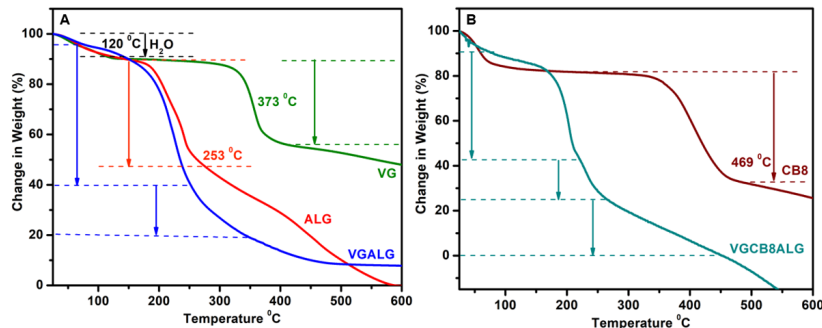


Figure 3. Thermo-gravimetric analysis showing the weight losses of VG (green), ALG (red), CB8 (dark red), VGALG (blue), and VGCB8ALG (dark cyan).

The weight loss percentage values at different temperatures were calculated from the TGA curves for all the samples to estimate the weight % of VG and CB8 in the modified alginates (Tables S2 in the Supporting Information). We divided the weight % by the molecular weight, giving us several moles. We then concluded the percentage by moles of VG (~20 %) in both alginate polymers. We also compared the number of moles of VG with CB8, which allowed us to conclude to 2:1 VG: CB8 interaction on the alginate surface, which agrees with other supramolecular architectures that contain CB8-complexed viologen dyes.^[18] Table S2 also includes the percentage of humidity, decomposition, complete organic degradation mass losses, and residues for ALG, VG, VGALG, CB8, and VGCB8ALG. It was observed that VGCB8ALG samples released a higher percentage of absorbed water than the ALG sample. This result indicates a more robust immobilization of water molecules because of the linking of ALG with VGCB8. The thermal stability of materials is manifested by a significant weight loss in the degradation stage when complete thermal degradation starts.

DSC data characterize the thermal behavior of individual ALG, VG, and CB8 in terms of their simple structure, hydrophilic properties, and association rate.^[29] The results confirm the linking of VG to ALG and its host-guest complexation to CB8 while linked to ALG. For the unmodified ALG, the DSC curve in Figure S3 in the Supporting Information shows an endothermic peak at 94.8°C followed by a strong exothermic peak around 288°C. Endothermic peaks were correlated with the loss of water associated with hydrophilic groups of the biopolymer. In contrast, exothermic peaks resulted from the decomposition of ALG, and subsequently, the decomposition of carbonaceous material occurred above 400°C. The DSC thermogram of VG unfolded an endothermic peak at 117°C attributed to the water release and an exothermic peak at 354°C due to the decomposition of viologen. Upon linking VG to ALG, the two exothermic peaks for ALG and VG were shifted to 232°C and 360°C, respectively. Table S3 in the Supporting Information presents the exothermic and endothermic peaks and the heat flow changes associated with each peak. The thermogram of CB8 shows an endothermic peak at 96°C, which is associated with the water release, and an exothermic peak at 387°C because of the decomposition of CB8. In contrast, the DSC of VGCB8ALG indicates the guest-host association as evidenced by the evolution of an endothermic peak at 387°C instead of an exothermic one in VGALG.

The particle size distribution (z-average hydrodynamic diameter (nm)) and surface charge (ζ potential (mV)) of VG, ALG, VGALG, and VGCB8ALG were studied by dynamic light scattering (DLS) and electrophoretic light scattering (ELS) as shown in Figure 4.

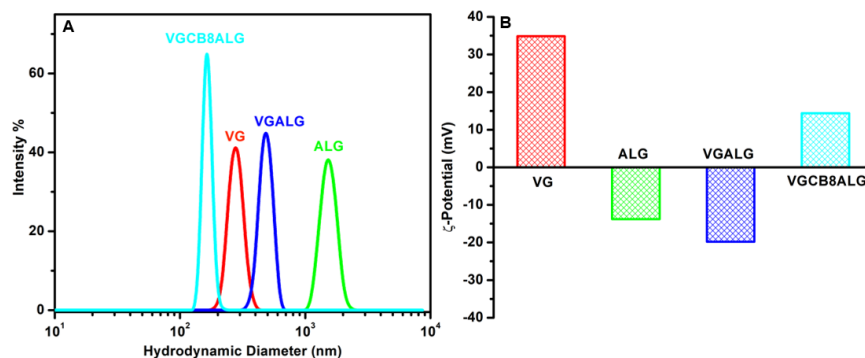


Figure 4. Particle size distribution of modified hydrogels and starting materials (A) and surface charge of different hydrogels and their components (B).

The samples were dissolved in methanol, and the size distribution and ζ potential were recorded. The measurement for ALG shows particles with a large size of 1540 nm. The ζ potential measured consistently higher value of -13.8 mV. The particle size measured for VG is 280 nm and has a relatively high ζ potential value of +34.9. As Figure 4 shows, the size distribution for VGALG revealed a particle size of 485 nm, and a ζ potential of -19.8 mV, indicating the robust binding of VG to ALG. The polydispersity index (PDI), a parameter for non-uniform particle distribution, shows a slightly higher result of 0.580, which also supports the non-uniform distribution of VGALG particles in the dissolution media. The measured size distribution for VGCB8ALG was 165 nm, and the ζ potential value shifted to +14.4 mV, indicating the guest-host interaction in VGCB8ALG.^[12] The manipulation in the size and charge of hydrogels upon the addition of CB8 explains the results of cellular internalization below.

Optical Properties (Functionalization, Encapsulation, Implementation for Cellular Uptake, and Rigidity Enhancement)

The solid UV–Visible spectra (Figure S4 in the Supporting Information) showed a slight difference in the band gap (0.06 eV) between the two hydrogels with the addition of CB8. Yet, both indicated distinct optical properties with onsets at approximately 700 nm compared to the published data for unmodified ALG with 212 and 271 nm peaks.^[30]

The excitation and emission spectra were recorded for the new hydrogels VGALG and VGCB8ALG in Figure 5 and found to be consistent with the solid UV–Visible data.

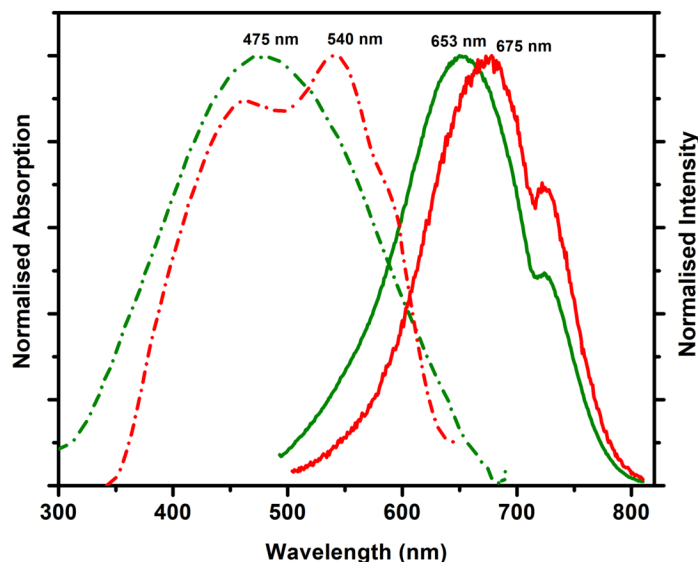


Figure 5. PL and PLE spectra in the solid state of the two modified hydrogels, VGALG (Green), measured with excitation wavelength at 475 nm and emission wavelength at 653 nm; and VGCB8ALG (Red), measured with excitation wavelength at 454 nm and emission wavelength at 675 nm.

The maxima shift from 475 to 540 nm and 653 to 675 nm in the excitation and emissions spectra, respectively, with the complexation of VG to CB8. The literature reveals entirely different PL and PLE spectra for VG or VGCB7^[21,25] in the solid state, and ALG is known to be non-emissive. The results confirm that the chemical engineering of ALG conceived novel solid PL/PLE properties of the new hydrogels enabling us to monitor their cellular uptake utilizing the flow cytometry technique. Moreover, the excited-state average lifetime values of the hydrogels in the solid state (see Methods section, Figure S5, and Table S4 in the Supporting Information) increased from 0.28 to 0.85 ns with the addition of CB8 because of the confinement effect.^[21,25-27] A more rigid biopolymer helps interpret the results of cellular internalization below.

Immunomodulatory Properties (Cellular Internalization)

The present study explored the potential effects of newly designed and prepared hydrogels on immunocompetent cells. Thus, the effects of VGALG and VGCB8ALG on the viability of peripheral blood mononuclear cells (PBMCs) from healthy donors using the WST-1 test (Figure S6 in the Supporting Information) were first evaluated. It was shown that the percentage of viable cells decreased only when cells were treated with VGALG, and not VGCB8ALG, at the maximum 1.8 mg/ml concentration used. We also evaluated the concentration of LDH in the culture medium after treatment with hydrogels to determine a possible cytotoxic effect (Figure S7 in the Supporting Information). LDH is released into the cell culture supernatant when the plasma membrane is damaged. Treatment of cells with both hydrogels resulted in cell damage only at high concentrations of 1.8 mg/ml. Therefore, hydrogels at concentrations of 0.18 mg/ml and below do not have a cytotoxic effect on PBMCs. That allows us to conclude that hydrogels under study have high biocompatibility characteristics and low toxic effects on immune cells. Following the literature, we expected a high safety profile from VGALG and VGCB8ALG since each component of the hydrogels, CB8,^[31] alginate,^[32,33] and viologen,^[34] is safe, biocompatible and has already been used separately to create similar hydrogels. The hydrogels (0.18 mg/mL) were then used for investigating the drug internalization to the PBMCs (CD3⁻ and CD3⁺T-lymphocytes) by flow cytometry (Figure S8 in the Supporting Information). PBMCs uptake of VGALG has no significant differences from the control (non-treated cells). In the case

of VGCB8ALG, internalization into CD3⁺ cells was low and was measured at about 6%, while the median uptake by T cells was 62%, which is ten times higher. Noticeably, CB8 is a critical factor for internalization into the T cells. In the case of CD14⁺ monocytes, internalization was carried out efficiently by both VGALG and VGCB8ALG (0.18 mg/mL), and no significant differences were observed between hydrogels (Figure S9 in the Supporting Information). The observed differences in internalization are associated with the mechanism of particle capture by various subpopulations of PBMCs; monocytes are capable of active phagocytosis of particles from the surrounding space, while T-lymphocytes, like most other body cells, do not have such a function.

Motivated by our results on the high level of internalization of the VGCB8ALG hydrogel into T-lymphocytes of healthy donors, we decided to evaluate the effect of hydrogels on human T-cell lymphoma 1301 cells. It was found that at all concentrations used, both hydrogels did not reduce the viability of 1301 cells at 24 and 72 hours of treatment (Figures S10 and S11 in the Supporting Information). Specifically, after 24 hours of treatment with 1301 hydrogels (Figure S10 in the Supporting Information), cell viability increased under the influence of VGCB8ALG compared to VGALG at a concentration of 1.8 mg/mL. Thus, VGCB8ALG at a high concentration can increase the number of viable cells in the culture, increasing the proliferation of the cells. Moreover, after 72 hours of treatment with 1301 hydrogels, the percentage of viable 1301 cells differed when treated with different concentrations of VGALG and VGCB8ALG (Figure S11 in the Supporting Information). For example, at a concentration of 1.8 mg/ml, there was an increase in viability in the VGCB8ALG group compared to VGALG. In contrast, treatment with VGALG increased the number of viable cells compared to treatment with VGCB8ALG at concentrations of 0.18 mg/ml and 0.018 mg/ml. Nonetheless, the two hydrogels do not have a toxic effect on 1301 human T-cell lymphoma cells with such long-term treatment for 72 hours. In summary, VGALG can enhance the proliferative activity of cells at average concentrations of 0.18 mg/ml and 0.018 mg/ml with long-term treatment for 72 h. Contrarily, VGCB8ALG increased the proliferative activity of these cells only at high concentrations (1.8 mg/ml) in culture for 24 and 72 hours. Following the viability results, we decided to evaluate the internalization of hydrogels at a concentration of 1.8 mg/ml by T-cell lymphoma cells at different treatment times (Figure S12 in the Supporting Information). The VGCB8ALG hydrogel was shown to be rapidly internalized by cells; after 1 hour, more than 80 percent of 1301 cells had absorbed the gel. After 24 and 72 hours, the percentage of internalized VGCB8ALG cells increased to more than 90%. Interestingly, VGALG was practically not absorbed by the cells at all times of treatment. To better explain this result, we evaluated the effect of hydrogel concentration on the uptake of T-cell lymphoma by the cell line (Figure 6). VGCB8ALG was efficiently taken up by cells at all concentrations used. The relative number of cells that took up VGCB8ALG varied with concentration, ranging from 99% at the highest to 15% at the lowest concentration. VGALG was poorly taken up by cells at all concentrations used.

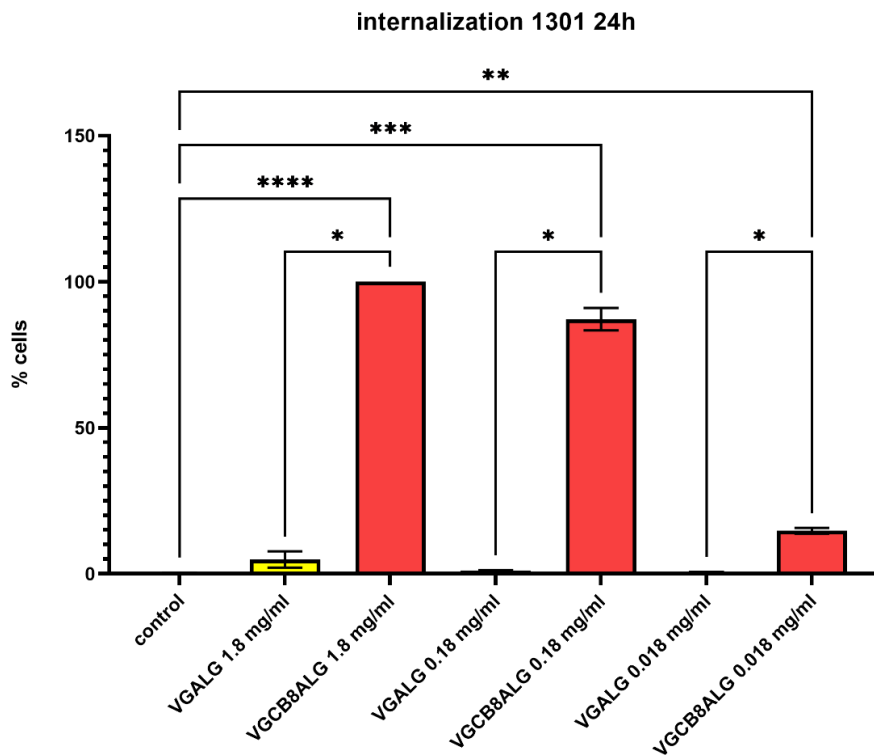


Figure 6. Evaluation of internalization of 1301 cells 24 hours of treatment by different concentrations of hydrogels (n=4).

To identify a possible pathway for hydrogel endocytosis into T-lymphocytes, 1301 cells were treated with 0.18 mg/ml VGCB8ALG together with inhibitors of various endocytosis pathways (Figure 7). As expected, exposure to hydrogels at four °C resulted in potent inhibition of endocytosis. The results showed a significant difference in uptake when inhibited with nystatin, thus suggesting caveolae-mediated endocytosis was preferred for VGCB8ALG.

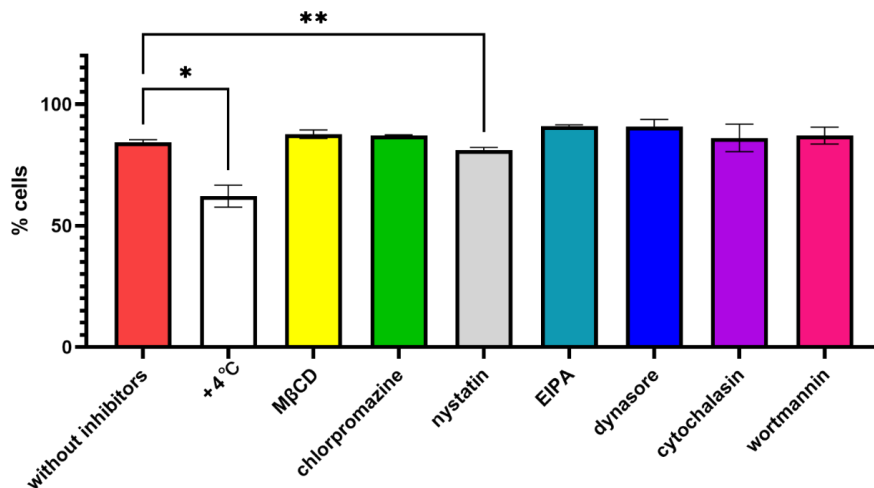


Figure 7. Effect of endocytosis inhibitors on the uptake of VGCB8ALG (0.18 mg/mL) by 1301 cells. (n=3)

To confirm our results, 1301 cells were treated with hydrogels for 24 hours, after which we performed fluorescence microscopy (Figure 8). Fluorescent microscopy images confirmed that VGCB8ALG compared to VGALG is strongly internalized into the cell and evenly distributed in it. VGCB8ALG is localized in the cytoplasm of cells.

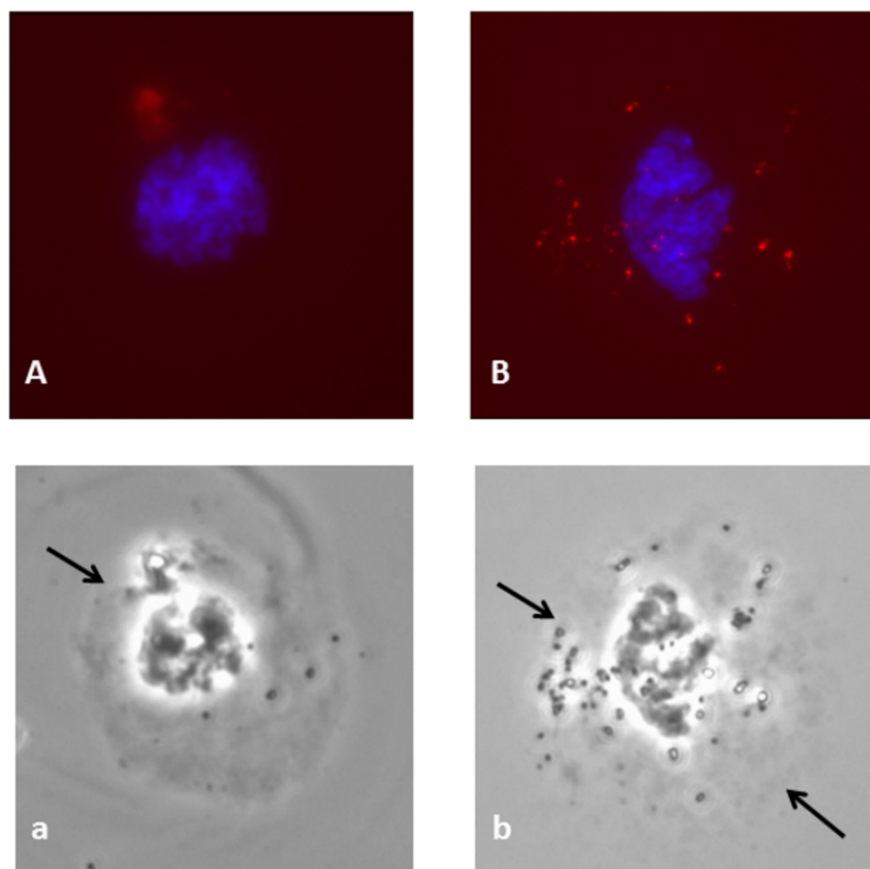


Figure 8. Upper cases (A, B) represent merged fluorescent images on the magnitude X1000. The red spots represent labeled hydrogel, and the nucleus is stained with DAPI (blue). (A) and (B) represent cellular uptake of hydrogel alone and in complex with CB8 correspondingly. Lower cases (a, b) represent the correspondent phase-contrast images on the magnitude X400 where arrows indicate the cytoplasm. The concentration of each hydrogel was 0.18 mg/mL.

Supramolecular Effects on Cellular Internalization (Role of Size, Charge, and Rigidity)

Overall, these data show that the modified ALG (drug carriers), by covalently anchoring VG tags into the polysaccharides that are readily non-covalently complexed to CB8 macromolecules have a distinct ability to cross leukemia cancer cells (Figure 9), giving a more explicit description of the cellular uptake mechanisms of supramolecular hydrogels in cancer therapy.

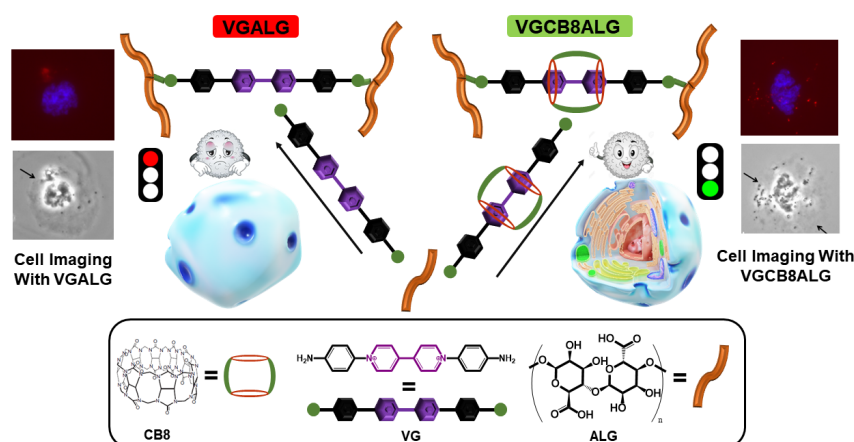


Figure 9. Schematic representation of blood cellular uptake of VGALG and VGCB8ALG hydrogels. Chemical structures of VG, ALG, and CB8 are also shown. The 2:1 binary complex of CB8 with the viologen dimers is not shown for simplicity.

As described in the introduction, employing supramolecular hydrogels based on polysaccharides for biomedical applications and utilizing cucurbituril macromolecules is not original and has received significant attention. It has also been described for various biological and clinical applications. Hydrogels are themselves a widely researched field of (bio)materials. They have been enormously reported, and the field is not novel.^[12] For example, hydrogel drug delivery has already implemented the host-guest association between cucurbit[7]uril (CB7) and cisplatin.^[35] Nonetheless, elucidating the effects of macromolecules on the mechanism of cellular uptake is still motivated.

The biocompatibility and low toxicity have been confirmed for the modified ALG in the present work. The translation of the unmodified ALG has already been explored in literature.^[36] The research concluded the significant role of size. Three different size-dependent mechanisms for cellular uptake were suggested. Oleoyl ALG ester nanoparticles whose sizes are 50, 120, or 730 nm enter the colon cancer cells via Clathrin-Mediated Endocytosis (CME), CvME, or micropinocytosis, respectively.^[36] From Figure 4, the CB8-modified ALG has a size that is 165 nm compared to 1540 nm for the undecorated ALG. The uptake mechanism was confirmed to be CvME which agrees with the literature. In another account, the authors highlighted the effect of charges on the uptake of nanoparticles. Because the lung cancer cell's surface has a negative charge, cationic cerium oxide nanoparticles^[37] were better internalized than neutrally or negatively charged ones, such as the cellular internalization of polyplexes, lipoplexes, and lipopolyplexes into a myoblast cell line.^[38] From Figure 4, the modified VGCB8ALG has a positive charge (viz. +14.4 mV) compared to the negatively charged VGALG (-19.8 mV) and thus was better internalized into leukemia cancer in agreement with those reports. The rigidity factor was demonstrated to modulate the type of cellular uptake, in which rigid nanoparticles of *N,N*-diethyl acrylamide, and 2-hydroxyethyl methacrylate cross-linked with *N,N*'-methylene-bis-acrylamide were better internalized to RAW 264.7 murine macrophage cells compared to soft nanoparticles.^[39] From Figure S5 in the Supporting Information, adding CB8 renders the modified hydrogels more rigid than VGALG. Thus, the increase in endocytosis is unsurprising. The exciting point remains the straightforward elucidation of how CB8 has modulated the cellular uptake, which can be further utilized for other clinical applications in the future.

Collectively these data unfold the factors that biomedical researchers need to consider (among others) to get more efficient drug delivery systems in cancer therapy that involves a macromolecular system or other drug vehicles. Although, nowadays, the field of application, material type, and drug loading need to be precisely selected and extensively studied, we envisage that the successful modulation of cellular internalization upon

the addition of CB8 on VGALG must have a wide impact in the broader research field and benefits similar cellular studies performed on other macrocycle-based biomaterials for other biomedical applications. The technology is patentable, which would then be of interest to international pharmaceutical companies for commercial development.

CONCLUSION

The present work offers a supramolecular strategy to modulate the cellular uptake and intracellular processing of drug delivery systems, paving the way for a more remarkable improvement in the development of drug therapeutics of alginates in cancer therapy. We showed that supramolecular encapsulation is the key required for the efficient delivery of a model drug system via CvME, as manifested in the substantial decrease in the size of the alginate hydrogels. The employment of a supramolecular approach to modify drug carriers is not new. Still, the results here confirm a distinct, unique modulation of the intracellular processing of alginate carriers, unfolding a thorough understanding of the macrocyclic effects on drug delivery compared to previous reports.

Supplementary Information The online version contains supplementary material available at **XXXXXX**.

Author Contributions

F.C.; optical data (UV, PL, TRPL) acquisition and analysis and writing the initial draft, V. P.; material characterization by FTIR, DLS, TGA, DSC, and NMR, P.L.; data analysis, M.B., A.A., O.B., M.B., and E.P.; clinical studies and contribute to manuscript writing, N.S. created the idea, conceptualization, supervision, and final manuscript writing. All authors have approved the final version of the manuscript.

Funding Sources

This study was supported by Grant 12R113 from UAE University.

Data availability: All relevant data are within the paper.

Declarations

Ethical approval The study was conducted according to the guidelines of the Declaration of Helsinki and approved by the Institutional Local Ethical Committee of the Research Institute of Fundamental and Clinical Immunology (protocol No. 141; 20 April 2023).

Consent to participate The participants consented.

Consent for publication The authors consented.

Conflict of interest The authors declare no competing interests.

AUTHOR INFORMATION

Corresponding Authors

n.saleh@uaeu.ac.ae; pashkina.e.a@yandex.ru.

ACKNOWLEDGMENTS

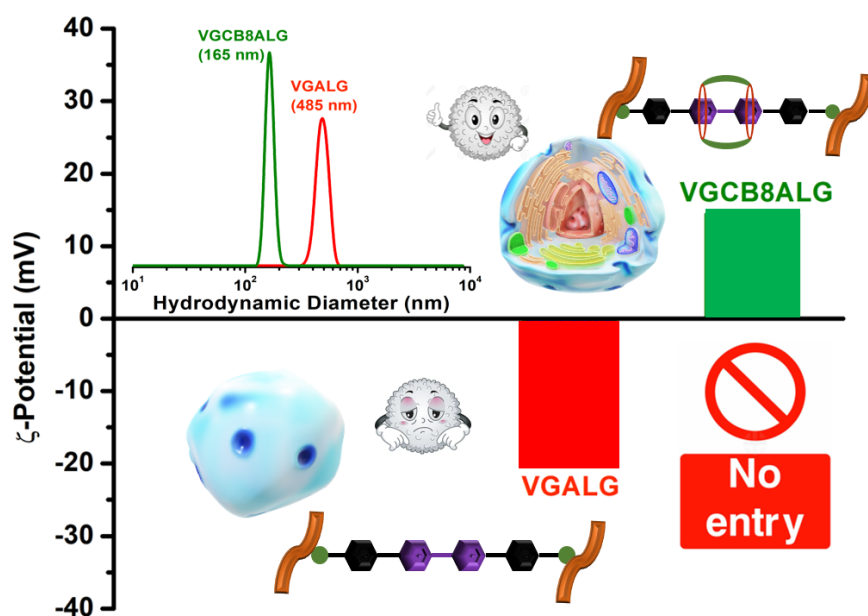
We thank the research program at United Arab Emirates University for financial grant number Grant 12R113 and the Russian Science Foundation for financial grant number 19-15-00192.

REFERENCES

[1] S. S. Soni, A. Alsasa, C. B. Rodell, *Front. Chem.* **2021** , *9* , 658548.

- [2] X. Yang, K. Varini, M. Godard, F. Gassiot, R. Sonnette, G. Ferracci, B. Pecqueux, V. Monnier, L. Charles, S. Maria, M. Hardy, O. Ouari, M. Khrestchatsky, P. Lécorché, G. Jacquot, D. Bardelang, *J. Med. Chem* **2023** , DOI <https://doi.org/10.1021/acs.jmedchem.3c00423>.
- [3] S. J. Barrow, S. Kasera, M. J. Rowland, J. Del Barrio, O. A. Scherman, *Chem. Rev.* **2015** , *115* , 12320–12406.
- [4] N. S. El-Sayed, S. Kamel, *Colloids. Interfaces.***2022** , *6* , 78.
- [5] Y. Gao, Y. Gao, Y. Ding, H. Tan, A. Zou, S. Li, *Chin. Chem. Lett.* **2021** , *32* , 949–953.
- [6] J. Skopinska-wisniewska, S. De la Flor, J. Kozłowska, *Int. J. Mol. Sci.* **2021** , *22* , 7402.
- [7] A. C. Madl, C. M. Madl, D. Myung, *ACS Macro Lett.***2020** , *9* , 619–626.
- [8] J. L. Mann, A. C. Yu, G. Agmon, E. A. Appel, *Biomater. Sci.* **2017** , *6* , 10–37.
- [9] J. Wang, Q. Li, S. Yi, X. Chen, *Soft Matt.* **2017** , *13* , 6490–6498.
- [10] Y. Liu, S. H. Hsu, *Front. Chem.* **2018** , *6* , 417832.
- [11] J. Omar, D. Ponsford, C. A. Dreiss, T. C. Lee, X. J. Loh, *Chem. Asian. J.* **2022** , *17* , e2022000.
- [12] A. Sohail, M. A. Alnaqbi, N. Saleh, *Macromole.***2019** , *52* , 9023–9031.
- [13] Y. Yao, Y. Wang, R. Zhao, L. Shao, R. Tang, F. Huang, *J. Mater. Chem. B* **2016** , *4* , 2691–2696.
- [14] F. Bray, A. Jemal, N. Grey, J. Ferlay, D. Forman, *Lancet. Oncol.* **2012** , *13* , 790–801.
- [15] D. DS, K. L, C. E, G. T, G. PA, H. TA, H. S, K. SS, L. AB, M. MJ, M. E, N. M, P. SK, R. LC, S. R, S. GK, S. DR, V.-C. MA, V. G, M. G, *J. Clin. Oncol.* **2016** , *34* , 3716.
- [16] D. Ma, G. Hettiarachchi, D. Nguyen, B. Zhang, J. B. Wittenberg, P. Y. Zavalij, V. Briken, L. Isaacs, *Nat. Chem.* **2012** , *4* , 503–510.
- [17] W. M. Nau, M. Florea, K. I. Assaf, *Isr. J. Chem.***2011** , *51* , 559–577.
- [18] J. Tian, T. Y. Zhou, S. C. Zhang, S. Aloni, M. V. Altöe, S. H. Xie, H. Wang, D. W. Zhang, X. Zhao, Y. Liu, Z. T. Li, *Nat. Commun.* **2014** , *5* , 5574.
- [19] L. Michaelis, E. S. Hill, *J. Gen. Physiol.***1933** , *16* , 859–873.
- [20] L. Striepe, T. Baumgartner, *Chem. – A. Euro. J.***2017** , *23* , 16924–16940.
- [21] G. Das, S. K. Sharma, T. Prakasam, F. Gandara, R. Mathew, N. Alkhatib, N. Saleh, R. Pasricha, J. C. Olsen, M. Baias, S. Kirmizialtin, R. Jagannathan, A. Trabolsi, *Commun. Chem.* **2019** , *2* , 1–9.
- [22] Y. Wang, M. Mortimer, C. H. Chang, P. A. Holden, *Nanomaterials* **2018** , *8* , 76.
- [23] E. Pashkina, A. Aktanova, I. Mirzaeva, E. Kovalenko, I. Andrienko, N. Knauer, N. Pronkina, V. Kozlov, *Int. J. Mol. Sci.***2021** , *22*
- [24] Z. Zeng, J. Xie, G. Luo, Z. Tao, Q. Zhang, *Beilstein Archives* **2020** , *2020* , 81.
- [25] F. Benyettou, K. Nchimi-Nono, M. Jouiad, Y. Lalatonne, I. Milosevic, L. Motte, J. C. Olsen, N. Saleh, A. Trabolsi, *Eur. J. Chem.* **2015** , *21* , 4607–4613.
- [26] M. Freitag, L. Gundlach, P. Piotrowiak, E. Galoppini, *J. Am. Chem. Soc.* **2012** , *134* , 3358–3366.
- [27] X. Yang, Q. Cheng, V. Monnier, L. Charles, H. Karoui, O. Ouari, D. Gimes, R. Wang, A. Kermagoret, D. Bardelang, *Angew. Chem., Int. Ed.* **2021** , *60* , 6617–6623.
- [28] S. Naz, H. Kara, S. T. H. Sherazi, A. Aljabour, F. N. Talpur, *RSC. Adv.* **2014** , *4* , 48419–48425.
- [29] N. H. Patil, P. V. Devarajan, *Drug. Deliv.***2016** , *23* , 429–436.

- [30] L. Motelica, D. Fikai, O. Oprea, A. Fikai, R. D. Trusca, E. Andronescu, A. M. Holban, *Pharmaceutics* **2021** , *13* , 1020.
- [31] T. Xiao, L. Xu, L. Zhou, X. Q. Sun, C. Lin, L. Wang, *J. Mater. Chem. B* **2019** , *7* , 1526–1540.
- [32] T. G. Barclay, C. M. Day, N. Petrovsky, S. Garg, *Carbohydr. Polym.* **2019** , *221* , 94–112.
- [33] C. R. Lynch, P. P. D. Kondiah, Y. E. Choonara, L. C. du Toit, N. Ally, V. Pillay, *Front Bioeng. Biotechnol.* **2020** , *8* , 228.
- [34] H. D. Correia, S. Chowdhury, A. P. Ramos, L. Guy, G. J. F. Demets, C. Bucher, *Polym. Int.* **2019** , *68* , 572–588.
- [35] R. Oun, J. A. Plumb, N. J. Wheate, *J. Inorg. Biochem.* **2014** , *134* , 100–105.
- [36] Q. Li, C. G. Liu, Y. Yu, *Carbohydr. Polym.* **2015** , *124* , 274–279.
- [37] A. Asati, S. Santra, C. Kaittanis, J. M. Perez, *ACS Nano* **2010** , *4* , 5321–5331.
- [38] L. Billiet, J. P. Gomez, M. Berchel, P. A. Jaffres, T. Le Gall, T. Montier, E. Bertrand, H. Cheradame, P. Guegan, M. Mevel, B. Pitard, T. Benvegna, P. Lehn, C. Pichon, P. Midoux, *Biomaterials* **2012** , *33* , 2980–2990.
- [39] X. Banquy, F. Suarez, A. Argaw, J. M. Rabanel, P. Grutter, J. F. Bouchard, P. Hildgen, S. Giasson, *Soft Matter.* **2009** , *5* , 3984–3991.



Graphical Abstract.

CB8 turns over the charge and decreases the size of VGALG hydrogel, enabling it to enter the blood cancer cells.